Mechanical Systems and Signal Processing 129 (2019) 381–393

Contents lists available at ScienceDirect

Mechanical Systems and Signal Processing

journal homepage: www.elsevier.com/locate/ymssp

# Model-independent PD-SMC method with payload swing suppression for 3D overhead crane systems

Menghua Zhang [a,*], Yongfeng Zhang [a], He Chen [b], Xingong Cheng [a]

[a] School of Electrical Engineering, University of Jinan, Jinan 250022, China
[b] School of Artificial Intelligence, Hebei University of Technology, Tianjin 300401, China

ARTICLE INFO

*Article history:*
Received 11 October 2018
Received in revised form 27 March 2019
Accepted 23 April 2019
Available online 6 May 2019

*Keywords:*
Underactuated overhead crane
PD-SMC
Swing suppression
Robustness
Lyapunov techniques
Schur complement

ABSTRACT

A model-independent control method, called proportional-derivative with sliding mode control method or PD-SMC in short, is designed for 3D overhead crane systems, where external disturbances, unmodeled and parametric uncertainties are present, to achieve simultaneous trolley positioning and payload swing suppression. One great benefit of the designed controller is its model-independent feature that can avoid requiring exact model knowledge. The proposed control method has the advantages of both simple structure of the PD control method and strong robustness of the SMC method. The PD control is utilized to stabilize the nominal model and the SMC is utilized to provide the robustness and to compensate the uncertainty and external disturbance of the controlled overhead crane systems. Moreover, to enhance the control performance of payload swing suppression and elimination, one additional term is introduced to the designed controller. Lyapunov techniques and Schur complement are utilized to analyze the asymptotically stable of the closed-loop system. Experimental results are illustrated to validate the effective and robustness of the new proposed control law.



## 1. Introduction

As powerful transportation tools, overhead cranes have been widely used in many fields, including factories, warehouses, construction sites [1,2]. As is well known, the two main control objectives of overhead crane systems are fast and accurate trolley positioning and rapid payload swing-elimination [3]. In practice, to flexible and simple the mechanical structure, no direct control force is imposed on the payload. Therefore, overhead crane is a highly underactuated nonlinear system whereas the number of the to-be-controlled system inputs is less than the degrees of freedom (DOFs). Such a system always suffers from external disturbances, parametric uncertainties, unmodeled uncertainties, cable flexibility, and considerable lack of actuators, which makes its control problems challenging and still open [4].

In the past couple of decades, many scholars have dedicated to studying the control issue of overhead cranes, and designed a series of meaningful controllers. The existing control methods can be roughly divided into two categories, i.e. open-loop control methods and closed-loop control methods, depending on whether or not the state feedback is required. More precisely, for open-loop controllers, by utilizing the coupling behavior between the trolley displacement and the payload swing, the trolley acceleration reference trajectories are planned; see, e.g., optimal control [5–7], motion planning [8–11], input shaping [12–15]. The planning trolley trajectories can reduce the payload swing while drive the trolley to the

* Corresponding author.
*E-mail address:* zhangmenghua@mail.sdu.edu.cn (M. Zhang).

https://doi.org/10.1016/j.ymssp.2019.04.046
0888-3270/

desired location. However, in the presence of uncertainties and external disturbances, the control performance of the open-loop control methods may be severely degraded. Many improved open loop techniques mainly in input shaping technique were proposed to cater the effect of uncertainties [16–18]. In such situation, closed-loop control methods, included visual-feedback-based control [19,20], partial feedback linearization control [21–25], energy/passivity-based control [26–29], differential-flatness-based control [30], model predictive control [31–33], state-observer-based control [34], delayed feedback control [35,36], adaptive control [26,37–40], nested saturation control [41], fuzzy logic control [42–44], neural networks [4,45], might work better.

When the working condition of overhead cranes is poor with severe external disturbances and unmodeled uncertainties, the overall control performance of the above mentioned control methods will be badly attenuated and might even lead to instability [46]. Hence, many researchers turn to sliding mode control (SMC) method, which is well known for its strong robustness. A series of SMC methods are proposed for underactuated overhead crane systems [39,46–51]. Unfortunately, for SMC method, it is difficult to calculate the equivalent complement where system parameters are required. Furthermore, most of the existing SMC methods require either approximations or linearizations to the original overhead crane dynamics, because it is very difficult to design an appropriate sliding surface for highly underactuated nonlinear systems. It is straightforward to design specific control laws ensuring that the system state converges to the designed sliding surface; however, proving the convergence of these state variables on the sliding surface is very difficult.

In our previous work [39], an adaptive proportional-derivative with sliding mode control law or APD-SMC in short, is proposed for 2D underactuated overhead crane systems. It is designed based on a critical assumption that the uncertain dynamics should satisfy "linearity-in-parameters" condition. Moreover, to prove the convergence of the state variables, the overhead crane model is linearized at the equilibrium point. When external and uncertainty exist, the state variables may move far away from the equilibrium point, leading to much difference between the original dynamics and the simplified dynamics. In this case, the control performance will be deeply affected and might even lead to instability.

To tackle the aforementioned problems, a model-independent PD-SMC method with payload swing suppression is proposed in this paper, which ensures that the state variables on the sliding surface converge to the desired ones even when the overhead cranes suffer from both external disturbances and unmodeled uncertainties. More precisely, to facilitate the subsequent controller development, the error model of overhead crane systems is first derived. Next, a PD with SMC scheme is proposed for 3D overhead crane systems. The proposed method replaces the estimated feedforward term of a standard SMC controller with a PD controller, avoiding requiring for knowledge of the overhead crane system dynamics. Furthermore, an additional term associated with the payload swing is introduced to the proposed method to enhance the control performance of payload swing suppression and elimination. The asymptotic stability of the equilibrium point and the state convergence are demonstrated by Lyapunov techniques and Schur complement. Finally, to verify the effective and robust of the designed controller, experimental results are provided.

The main contribution of this paper can be concluded as follows:

1. The proposed control method successfully proves the state convergence on the sliding surface without requiring linearizing the original nonlinear dynamics or neglecting partial nonlinear terms. The primary advantage is that, even if the system state is far from the equilibrium point, the proposed control method can still work well.
2. The design control law is model free, i.e. it involves no system-parameter-related terms (e.g. cable length, trolley/payload/bridge mass, friction-related parameters), which makes it robust with uncertain/unknown system parameters.
3. In comparison with most currently available closed-loop control methods, the proposed control law has a simpler structure, therefore, it is easy to implement for real applications.

The remaining parts of this paper are arranged as follows. In Section II, the nonlinear dynamics of 3D overhead crane systems and the proposed PD-SMC with payload sway reduction are discussed. The stability analysis is presented in Section III. In Section IV, experimental results are presented to validate the feasibility and effectiveness of the designed controller. In Section V, some concluding remarks are drawn.

## 2. Dynamic model and designed PD-SMC method with payload swing suppression

In this section, the dynamical equations of motion for 3D overhead crane systems are provided and then design the PD-SMC method with payload sway reduction.

The dynamical equations for a 3D overhead crane system are shown as follows (see Fig. 1) [10,20,23,24,27,29,47]:

$$(M_x + m_p)\ddot{x} + m_p l\ddot{\theta}_x C_x C_y - m_p l\ddot{\theta}_y S_x S_y - 2m_p l\dot{\theta}_x\dot{\theta}_y C_x S_y - m_p l\dot{\theta}_x^2 S_x C_y - m_p l\dot{\theta}_y^2 S_x C_y = F_x - f_{rx}, \tag{1}$$

$$(M_y + m_p)\ddot{y} - m_p l\ddot{\theta}_y C_y + m_p l\dot{\theta}_y^2 S_y = F_y - f_{ry}, \tag{2}$$

$$m_p\ddot{x}lC_x C_y + m_p l^2\ddot{\theta}_x C_y^2 - 2m_p l^2\dot{\theta}_x\dot{\theta}_y C_y S_y + m_p g l S_x C_y = 0, \tag{3}$$

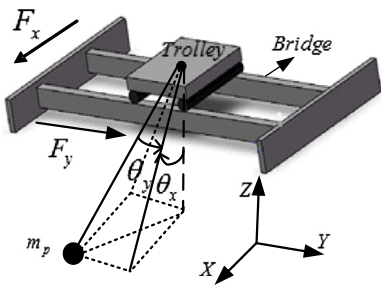


**Fig. 1.** 3D overhead crane system.

$$-m_p\ddot{x}lS_xS_y - m_p\ddot{y}lC_y + m_pl^2\ddot{\theta}_y + m_pl^2\dot{\theta}_x^2C_yS_y + m_pglC_xS_y = 0, \tag{4}$$

where $M_x$ stands for the trolley mass, $M_y$ is the sum of the trolley mass and the bridge mass, $m_p$ represents the payload mass, $l$ and $g$ denote the rope length and the gravitational constant, respectively, $x$ and $y$ represent the trolley displacements along the $X$ and the $Y$ axis, respectively, $\theta_x$ and $\theta_y$ are used to depict the payload's swing, $F_x$ and $F_y$ represent the control inputs imposed on the trolley along the $X$ and the $Y$ axis, respectively, $S_x$, $S_y$, $C_x$ and $C_y$ are the abbreviations of $\sin\theta_x$, $\sin\theta_y$, $\cos\theta_x$ and $\cos\theta_y$, respectively, $f_{rx}$ and $f_{ry}$ denote the nonlinear friction along the $X$ and the $Y$ axis, respectively. After a lot of experimental measurements, the following friction models are selected as [26–29,39,49]:

$$f_{rx} = f_{rox}\tanh\left(\frac{\dot{x}}{\varepsilon_x}\right) - k_{rx}|\dot{x}|\dot{x}, \tag{5}$$

$$f_{ry} = f_{roy}\tanh\left(\frac{\dot{y}}{\varepsilon_y}\right) - k_{ry}|\dot{y}|\dot{y}, \tag{6}$$

where $f_{rox}$, $f_{roy}$, $\varepsilon_x$, $\varepsilon_y$, $k_{rx}$, and $k_{ry}$ are friction-related coefficients.

From (3) and (4), it can be easily concluded that

$$\ddot{\theta}_x = -\frac{C_x}{lC_y}\ddot{x} + \frac{2S_y}{C_y}\dot{\theta}_x\dot{\theta}_y - \frac{gS_x}{lC_y}, \tag{7}$$

$$\ddot{\theta}_y = \frac{S_xS_y}{l}\ddot{x} + \frac{C_y}{l}\ddot{y} - C_yS_y\dot{\theta}_x^2 - \frac{g}{l}C_xS_y. \tag{8}$$

It follows from (1)–(2) and (7)–(8) that

$$\left(M_x + m_pS_x^2C_y^2\right)\ddot{x} - m_pS_xS_yC_y\ddot{y} - m_plS_xC_yC_y^2\dot{\theta}_x^2 - m_pl\dot{\theta}_y^2S_xC_y - m_pgC_xS_xC_y^2 + f_{rx} = F_x, \tag{9}$$

$$-m_pS_xS_yC_y\ddot{x} + \left(M_y + m_pS_y^2\right)\ddot{y} + m_plS_yC_y^2\dot{\theta}_x^2 + m_pl\dot{\theta}_y^2S_y + m_pgC_xS_yC_y + f_{ry} = F_y. \tag{10}$$

First of all, the following trolley positioning error signals are introduced as:

$$e_x = x - p_{dx} \Rightarrow \dot{e}_x = \dot{x},\ \ddot{e}_x = \ddot{x}, \tag{11}$$

$$e_y = y - p_{dy} \Rightarrow \dot{e}_y = \dot{y} \Rightarrow \ddot{e}_y = \ddot{y}, \tag{12}$$

where $p_{dx}$ and $p_{dy}$ stand for the trolley desired location along the $X$ and the $Y$ axis.

It can be obtained from (9)–(12) that

$$\left(M_x + m_pS_x^2C_y^2\right)\ddot{e}_x - m_pS_xS_yC_y\ddot{e}_y - m_plS_xC_y^3\dot{\theta}_x^2 - m_pl\dot{\theta}_y^2S_xC_y - m_pgC_xS_xC_y^2 + f_{rx} = F_x, \tag{13}$$

$$-m_pS_xS_yC_y\ddot{e}_x + \left(M_y + m_pS_y^2\right)\ddot{e}_y + m_plS_yC_y^2\dot{\theta}_x^2 + m_pl\dot{\theta}_y^2S_y + m_pgC_xS_yC_y + f_{ry} = F_y. \tag{14}$$

To be concise, the error dynamics can be rewritten into a compact form:

$$\boldsymbol{M}(\boldsymbol{e})\ddot{\boldsymbol{e}} + \boldsymbol{F}_d = \boldsymbol{u}, \tag{15}$$

where $\boldsymbol{e} = [e_x\ e_y]^T \in \mathbb{R}^2$ denotes the positioning error vector, $\boldsymbol{u} = [F_x\ F_y]^T \in \mathbb{R}^2$ stand for the control input vector, $\boldsymbol{M}(\boldsymbol{e}) \in \mathbb{R}^{2\times2}$, $\boldsymbol{F}_d \in \mathbb{R}^2$ are the following auxiliary matrix and vector:

$$\boldsymbol{M}(\boldsymbol{e}) = \begin{bmatrix} M_x + m_p S_x^2 C_y^2 & -m_p S_x S_y C_y \\ -m_p S_x S_y C_y & M_y + m_p S_y^2 \end{bmatrix}, \boldsymbol{F}_d = \begin{bmatrix} -m_p l S_x C_y^3 \dot{\theta}_x^2 - m_p l \dot{\theta}_y^2 S_x C_y - m_p g C_x S_x C_y^2 + f_{rx} \\ m_p l S_y C_y^2 \dot{\theta}_x^2 + m_p l \dot{\theta}_y^2 S_y + m_p g C_x S_y C_y + f_{ry} \end{bmatrix}, \tag{16}$$

respectively.

Motivated in part by the static torque methodology [52,53], by introducing a positive diagonal matrix $\Lambda \in \mathbb{R}^{2\times 2}$, we can rewrite (15) into

$$\begin{aligned} \boldsymbol{u} &= \Lambda \ddot{\boldsymbol{e}} + (\boldsymbol{M}(\boldsymbol{e}) - \Lambda)\ddot{\boldsymbol{e}} + \boldsymbol{F}_d \\ &= \Lambda \ddot{\boldsymbol{e}} + \boldsymbol{P}_d. \end{aligned} \tag{17}$$

The expressions of $\Lambda \in \mathbb{R}^{2\times 2}$ and $\boldsymbol{P}_d \in \mathbb{R}^2$ are given as follows:

$$\begin{aligned} &\Lambda = \begin{bmatrix} \Lambda_1 & 0 \\ 0 & \Lambda_2 \end{bmatrix}, \\ &\boldsymbol{P}_d = (\boldsymbol{M}(\boldsymbol{e}) - \Lambda)\ddot{\boldsymbol{e}} + \boldsymbol{F}_d \\ &= \begin{bmatrix} \left\{ \begin{array}{c} \left(M_x + m_p S_x^2 C_y^2 - \Lambda_1\right)\ddot{e}_x - m_p S_x S_y C_y \ddot{e}_y \end{array} \right\} \\ \left\{ \begin{array}{c} -m_p l S_x C_y^3 \dot{\theta}_x^2 - m_p l \dot{\theta}_y^2 S_x C_y - m_p g C_x S_x C_y^2 + f_{rx} \end{array} \right\} \\ \left\{ \begin{array}{c} -m_p S_x S_y C_y \ddot{e}_x + \left(M_y + m_p S_y^2 - \Lambda_2\right)\ddot{e}_y \end{array} \right\} \\ \left\{ \begin{array}{c} +m_p l S_y C_y^2 \dot{\theta}_x^2 + m_p l \dot{\theta}_y^2 S_y + m_p g C_x S_y C_y + f_{ry} \end{array} \right\} \end{bmatrix}. \end{aligned} \tag{18}$$

The following assumptions concerning the further stability analysis are given as follows.

**Assumption 1.** Boundedness: There exists a positive constant $\sigma$ such that:

$$\left|\dot{\theta}_x \ddot{\theta}_x + \dot{\theta}_y \ddot{\theta}_y\right| < \sigma. \tag{19}$$

**Assumption 2.** The payload swing angles satisfy [26–29,39,49]:

$$-\pi/2 < \theta_x < \pi/2, \ -\pi/2 < \theta_y < \pi/2, \tag{20}$$

respectively.

**Remark 1.** In practice, to guarantee smooth transportation and safety, the accelerations of the trolley usually satisfy $\ddot{x}, \ \ddot{y} < g$ [42], where g denotes gravitational acceleration. Under such circumstances, the payload swing angles are usually kept within $\theta_{x\max}, \ \theta_{y\max} \leq 10^\circ$; Moreover, the angular velocities and the angular accelerations are kept within permitted ranges [11,14,15,39]. Therefore, it is reasonable to assume $\left|\dot{\theta}_x \ddot{\theta}_x + \dot{\theta}_y \ddot{\theta}_y\right| < \sigma$.

Then, the following sliding surface is introduced as

$$\boldsymbol{s} = \boldsymbol{e} + \boldsymbol{\lambda}\dot{\boldsymbol{e}}, \tag{21}$$

where $\boldsymbol{\lambda} \in \mathbb{R}^{2\times 2}$ denotes the positive diagonal sliding surface slope matrix.

With (17) and (21), the following robust PD-SMC method is proposed as:

$$\boldsymbol{u} = -\boldsymbol{K}_p \boldsymbol{e} - \boldsymbol{K}_d \dot{\boldsymbol{e}} - \boldsymbol{K}_s \mathrm{sgn}(\boldsymbol{s}), \tag{22}$$

where $\boldsymbol{K}_p \in \mathbb{R}^{2\times 2}$, $\boldsymbol{K}_d \in \mathbb{R}^{2\times 2}$ stand for the positive diagonal control gain matrix, $\boldsymbol{K}_s \in \mathbb{R}^{2\times 2}$ represents the positive diagonal SMC gain matrix, $\mathrm{sgn}(\cdot)$ is the sign function, whose expression is provided as follows:

$$\mathrm{sgn}(*) = \begin{cases} 1 \text{ if } * > 0 \\ 0 \text{ if } * = 0 \\ -1 \text{ if } * < 0 \end{cases} \tag{23}$$

Although the asymptotically stable of the closed-loop equilibrium point can be proved by using (22), the information of the payload swing angles is not directly utilized. To overcome the abovementioned drawback, the final PD-SMC method with payload sway reduction is presented as follows:

$$\boldsymbol{u} = -\boldsymbol{K}_p \boldsymbol{e} - \boldsymbol{K}_d \dot{\boldsymbol{e}} - \boldsymbol{K}_s \mathrm{sgn}(\boldsymbol{s}) - \boldsymbol{K}_\theta \left(\dot{\theta}_x^2 + \dot{\theta}_y^2\right)\dot{\boldsymbol{e}} = -\boldsymbol{K}_p \boldsymbol{e} - \left(\boldsymbol{K}_d + \boldsymbol{K}_\theta \left(\dot{\theta}_x^2 + \dot{\theta}_y^2\right)\right)\dot{\boldsymbol{e}} - \boldsymbol{K}_s \mathrm{sgn}(\boldsymbol{s}). \tag{24}$$

where $\boldsymbol{K}_\theta \in \mathbb{R}^{2\times 2}$ is the positive diagonal control gain matrix.

To avoid chattering phenomenon associated with SMC method, we introduce a hyperbolic tangent function to replace the sign function as follows:

$$\boldsymbol{u} = -\boldsymbol{K}_p\boldsymbol{e} - \left(\boldsymbol{K}_d + \boldsymbol{K}_\theta\left(\dot{\theta}_x^2 + \dot{\theta}_y^2\right)\right)\dot{\boldsymbol{e}} - \boldsymbol{K}_s\tanh(\boldsymbol{s}) = \boldsymbol{u}_{pd} + \boldsymbol{u}_{swing} + \boldsymbol{u}_{smc}. \tag{25}$$

where $\boldsymbol{u}_{pd} = -\boldsymbol{K}_p\boldsymbol{e} - \boldsymbol{K}_d\dot{\boldsymbol{e}}$ represents the PD component, $\boldsymbol{u}_{swing} = -\boldsymbol{K}_\theta\left(\dot{\theta}_x^2 + \dot{\theta}_y^2\right)\dot{\boldsymbol{e}}$ stands for the swing-elimination component, and $\boldsymbol{u}_{smc} = -\boldsymbol{K}_s\tanh(\boldsymbol{s})$ denotes the SMC component.

Fig. 2 shows a control block diagram for the proposed PD-SMC method with payload swing suppression.

Before starting the stability analysis of the proposed PD-SMC law, the following proposition is given.

**Preposition:** Let matrix $\boldsymbol{Q}$ be a symmetric matrix express as

$$\boldsymbol{Q} = \begin{bmatrix} \boldsymbol{A} & \boldsymbol{B} \\ \boldsymbol{B}^T & \boldsymbol{C} \end{bmatrix}. \tag{26}$$

Let $\boldsymbol{S}$ be Schur complement [54–56] of matrix $\boldsymbol{A}$ in $\boldsymbol{Q}$, that is

$$\boldsymbol{S} = \boldsymbol{C} - \boldsymbol{B}^T\boldsymbol{A}^{-1}\boldsymbol{B}. \tag{27}$$

Then the matrix $\boldsymbol{Q}$ is positive definite if and only if $\boldsymbol{A}$ and $\boldsymbol{S}$ are both positive definite [54–56], i.e.

$$\textit{If} \quad \boldsymbol{A} > 0, \quad \text{and} \quad \boldsymbol{S} > 0, \quad \text{then } \boldsymbol{Q} > 0. \tag{28}$$

## 3. Stability analysis

The following theorem summarizes the main results.

**Theorem 1.** The proposed PD-SMC law described by (25) can drive the trolley to the desired position and eliminate the payload swings in the following manner:

$$\lim_{t\to\infty}\left[x\ y\ \dot{x}\ \dot{y}\ \theta_x\ \theta_y\ \dot{\theta}_x\ \dot{\theta}_y\right]^T = \left[p_{dx}\ p_{dy}\ 0\ 0\ 0\ 0\ 0\ 0\right]^T, \tag{29}$$

if the following conditions are satisfied:

$$\begin{cases} \boldsymbol{K}_p > \sigma\boldsymbol{K}_\theta \\ \boldsymbol{K}_d > \boldsymbol{\lambda}^{-1}\Lambda \\ \boldsymbol{K}_s > \| \boldsymbol{P}_d \| \end{cases}. \tag{30}$$

**Remark 2.** Due to the nature of Lyapunov-based controller design techniques, condition (30) is conservative, which is merely sufficient condition to guarantee the stability. Thus, when implementing the designed controller, we can moderately relax these gain conditions.

To prove the stability of the proposed PD-SMC method, we prove that the following matrix $\boldsymbol{L}$ is positive definite:

$$\boldsymbol{L} = \begin{bmatrix} \boldsymbol{K}_d\ \Lambda \\ \Lambda\ \lambda\Lambda \end{bmatrix}. \tag{31}$$

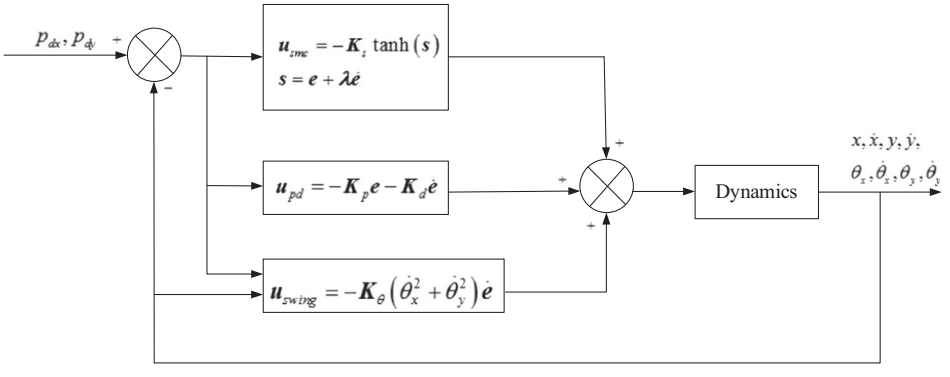


**Fig. 2.** Block diagram for the proposed PD-SMC method with payload swing suppression.

From (30), it can be obtained that

$$\begin{cases} \boldsymbol{K}_d > 0 \\ \boldsymbol{S} = \boldsymbol{\lambda}\Lambda - \boldsymbol{K}_d^{-1}\Lambda^T\Lambda > 0 \end{cases} \Rightarrow \boldsymbol{L} > 0. \tag{32}$$

The following Lyapunov candidate function is defined as:

$$V_{all}(t) = [\boldsymbol{e} \quad \dot{\boldsymbol{e}}]\boldsymbol{L}\begin{bmatrix} \boldsymbol{e} \\ \dot{\boldsymbol{e}} \end{bmatrix} + \frac{1}{2}\boldsymbol{\lambda}\mathbf{K}_p\boldsymbol{e}^{\,T}\boldsymbol{e} + \frac{1}{2}\boldsymbol{K}_\theta\left(\dot{\theta}_x^2 + \dot{\theta}_y^2\right)\boldsymbol{e}^{\,T}\boldsymbol{e}. \tag{33}$$

The time derivative of (33) is given by:

$$\begin{aligned} \dot{V}_{all}(t) &= [\boldsymbol{e} \quad \dot{\boldsymbol{e}}]\begin{bmatrix} \boldsymbol{K_d} & \Lambda \\ \Lambda & \boldsymbol{\lambda}\Lambda \end{bmatrix}\begin{bmatrix} \dot{\boldsymbol{e}} \\ \ddot{\boldsymbol{e}} \end{bmatrix} + \boldsymbol{\lambda}\mathbf{K}_p\boldsymbol{e}^{\,T}\dot{\boldsymbol{e}} + \boldsymbol{K}_\theta\left(\dot{\theta}_x^2 + \dot{\theta}_y^2\right)\boldsymbol{e}^{\,T}\dot{\boldsymbol{e}} + \boldsymbol{K}_\theta\left(\dot{\theta}_x\ddot{\theta}_x + \dot{\theta}_y\ddot{\theta}_y\right)\boldsymbol{e}^{\,T}\boldsymbol{e} \\ &= [\boldsymbol{e} \quad \dot{\boldsymbol{e}}]\begin{bmatrix} \boldsymbol{K_d}\dot{\boldsymbol{e}} + \Lambda\ddot{\boldsymbol{e}} \\ \Lambda\dot{\boldsymbol{e}} + \boldsymbol{\lambda}\Lambda\ddot{\boldsymbol{e}} \end{bmatrix} + \boldsymbol{\lambda}\mathbf{K}_p\boldsymbol{e}^{\,T}\dot{\boldsymbol{e}} \\ &= [\boldsymbol{e} \quad \dot{\boldsymbol{e}}]\begin{bmatrix} \boldsymbol{K_d}\dot{\boldsymbol{e}} - \boldsymbol{K}_p\boldsymbol{e} - \left(\boldsymbol{K}_d + \boldsymbol{K}_\theta\left(\theta_x^2 + \theta_y^2\right)\right)\dot{\boldsymbol{e}} - \boldsymbol{K}_s sign(\boldsymbol{s}) + \boldsymbol{P}_d \\ \Lambda\dot{\boldsymbol{e}} + \boldsymbol{\lambda}\left(-\boldsymbol{K}_p\boldsymbol{e} - \left(\boldsymbol{K}_d + \boldsymbol{K}_\theta\left(\theta_x^2 + \theta_y^2\right)\right)\dot{\boldsymbol{e}} - \boldsymbol{K}_s sign(\boldsymbol{s}) + \boldsymbol{P}_d\right) \end{bmatrix} + \boldsymbol{\lambda}\mathbf{K}_p\boldsymbol{e}^{\,T}\dot{\boldsymbol{e}} \\ &= \boldsymbol{s}^T(\boldsymbol{P}_d - \boldsymbol{K}_s\mathrm{sgn}(\boldsymbol{s})) - \left(\boldsymbol{K}_p - \boldsymbol{K}_\theta\left(\dot{\theta}_x\ddot{\theta}_x + \dot{\theta}_y\ddot{\theta}_y\right)\right)\boldsymbol{e}^T\boldsymbol{e} - (\boldsymbol{\lambda}\boldsymbol{K}_d - \Lambda)\dot{\boldsymbol{e}}^T\dot{\boldsymbol{e}} - \boldsymbol{\lambda}\boldsymbol{K}_\theta\left(\theta_x^2 + \theta_y^2\right)\dot{\boldsymbol{e}}^T\dot{\boldsymbol{e}}. \end{aligned} \tag{34}$$

The following inequality holds from (30):

$$\boldsymbol{s}^T\boldsymbol{K}_s\mathrm{sgn}(\boldsymbol{s}) = \|\,\boldsymbol{s}\,\|\boldsymbol{K}_s \geq \|\,\boldsymbol{s}\,\|\|\,\boldsymbol{P}_d\,\| \Rightarrow \boldsymbol{s}^T(\boldsymbol{P}_d - \boldsymbol{K}_s\mathrm{sgn}(\boldsymbol{s})) \leq 0. \tag{35}$$

Therefore, from (30) and (35), (34) can be rewritten as

$$\dot{V}_{all}(t) \leq -(\boldsymbol{K}_p - \sigma\boldsymbol{K}_\theta)\boldsymbol{e}^T\boldsymbol{e} - (\boldsymbol{\lambda}\boldsymbol{K}_d - \Lambda)\dot{\boldsymbol{e}}^T\dot{\boldsymbol{e}} - \boldsymbol{\lambda}\boldsymbol{K}_\theta\left(\dot{\theta}_x^2 + \dot{\theta}_y^2\right)\dot{\boldsymbol{e}}^T\dot{\boldsymbol{e}} \leq 0. \tag{36}$$

From (36), one can see that $\dot{V}_{all}(t) \leq 0$. The equality $\dot{V}_{all}(t) = 0$ is satisfied if and only if $\boldsymbol{e} = 0$, $\dot{\boldsymbol{e}} = 0$. Since the Lyapunov candidate function $V_{all}(t)$ is positive definite, and $\dot{V}_{all}(t)$ is a negative definite function, the 3D overhead crane system controlled by the designed PD-SMC controller is asymptotically stable [57]. When the state reaches the sliding manifold, the tracking error and derivative asymptotically converge to zeros [55], in the sense that

$$\boldsymbol{e} = 0, \quad \dot{\boldsymbol{e}} = 0. \tag{37}$$

From (37), (21), (11), (12), (5) and (6) it can be easily concluded that

$$s = 0,\ e_x = \ e_y = 0,\ \dot{e}_x = \dot{x} = 0,\ \dot{e}_y = \dot{y} = 0,\ \ddot{e}_x = \ddot{x} = 0,\ \ddot{e}_y = \ddot{y} = 0,\ f_{rx} = f_{ry} = 0. \tag{38}$$

Substituting the results of (37) and (38) into (25) yields

$$\boldsymbol{u} = 0 \Rightarrow F_x = 0,\ F_y = 0. \tag{39}$$

Next, we further illustrate that $\theta_x = 0$, $\theta_y = 0$, $\dot{\theta}_x = 0$, and $\dot{\theta}_y = 0$. By using (37) and (39), after some arrangements, (13) can be reduced as:

$$-m_p l S_x C_y^3\dot{\theta}_x^2 - m_p l\dot{\theta}_y^2 S_x C_y - m_p g C_x S_x C_y^2 = 0. \tag{40}$$

From (40), we are led to:

$$S_x\left(lC_y^2\dot{\theta}_x^2 + l\dot{\theta}_y^2 + gC_xC_y\right) = 0. \tag{41}$$

From assumption 2, we know that $C_x > 0$ and $C_y > 0$. Hence, it is obtained from (41) that

$$S_x = 0 \Rightarrow \theta_x = 0,\ \dot{\theta}_x = 0. \tag{42}$$

In a similar way, substituting (38) and (39) into (14) yields

$$m_p l S_y C_y^2\dot{\theta}_x^2 + m_p l\dot{\theta}_y^2 S_y + m_p g C_x S_y C_y = 0. \tag{43}$$

After some arrangements, it is concluded that

$$S_y\left(lC_y^2\dot{\theta}_x^2 + l\dot{\theta}_y^2 + gC_xC_y\right) = 0. \tag{44}$$

Again, using $C_x > 0$ and $C_y > 0$, it is obtained that

$$S_y = 0 \Rightarrow \theta_y = 0,\ \dot{\theta}_y = 0. \tag{45}$$

After gathering the results of (38), (42), and (45), Theorem 1 is proven.

## 4. Experimental results

In this section, two groups of hardware experimental tests are provided to validate the control performance of the designed PD-SMC method on a hardware overhead crane setup (from College of Engineering, Qufu Normal University, see Fig. 3). Specifically, in the first group, the proposed control method is compared with some existing methods. The second group verifies the robustness of the designed controller with respect to different external disturbances and uncertainties. It should be pointed out that, the friction between the trolley and the bridge is not compensated for the proposed PD-SMC method throughout the experiments.

The physical parameters for the crane setup are set as

$$M_x = 6.157 \text{ kg},\ M_y = 15.594 \text{ kg},\ l = 0.6 \text{ m},\ m_p = 1 \text{ kg},\ g = 9.8 \text{ m/s}^2.$$

The friction-related parameters for (5)–(6) are identified as follows:

$$f_{rox} = 23.652,\ \varepsilon_x = 0.01,\ k_{rx} = -0.8,$$
$$f_{roy} = 20.371,\ \varepsilon_y = 0.01,\ k_{ry} = -1.4.$$

The trolley desired location is

$$p_{dx} = 0.4 \text{ m},\ p_{dy} = 0.3 \text{ m}.$$

By trial and error, the control gains for the designed PD-SMC method are chosen as follows:

$$\boldsymbol{K}_p = \begin{bmatrix} 15.6 & 0 \\ 0 & 13.8 \end{bmatrix}, \boldsymbol{K}_d = \begin{bmatrix} 6.3 & 0 \\ 0 & 3.8 \end{bmatrix}, \boldsymbol{K}_\theta = \begin{bmatrix} 1.3 & 0 \\ 0 & 1.8 \end{bmatrix}, \boldsymbol{K}_s = \begin{bmatrix} 2.5 & 0 \\ 0 & 3.5 \end{bmatrix}, \boldsymbol{\lambda} = \begin{bmatrix} 1 & 0 \\ 0 & 1 \end{bmatrix}.$$

**Remark 3.** For real-time experimental implementation in the overhead crane testbed, the trolley displacements $x(t)$ and $y(t)$ are measured by the coaxial encoders embedded in the motors, the payload swing angles $\theta_x(t)$ and $\theta_y(t)$ are derived by incremental angle encoders. $\dot{x}(t)$, $\dot{y}(t)$, $\dot{\theta}_x(t)$ and $\dot{\theta}_y(t)$ are estimated by performing numerical difference operations to $x(t)$, $y(t)$, $\theta_x(t)$, and $\theta_y(t)$ along with low-pass filters.

### 4.1. Experiment 1

In this group, by comparing the proposed method with the LQR control method, the energy coupling output feedback (ECOF) control method [27], and the adaptive proportional-derivative sliding mode control (APD-SMC) method proposed in [39], the control performance of our designed controller is illustrated. To facilitate the understanding, the expressions of the abovementioned three controllers are given as follows. It should be pointed out that the APD-SMC method is proposed for 2D overhead crane systems, and thus, the expression of the controller is modified correspondingly for experiment implementation.

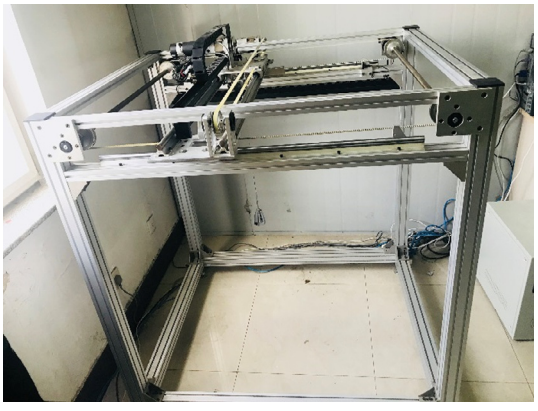

**Fig. 3.** Overhead crane experimental testbed.

1) LQR control method

$$\begin{aligned} F_x &= -k_{1x}(x - p_{dx}) - k_{2x}\dot{x} - k_{3x}\theta_x - k_{4x}\dot{\theta}_x, \\ F_y &= -k_{1y}(y - p_{dy}) - k_{2y}\dot{y} - k_{3y}\theta_y - k_{4y}\dot{\theta}_y, \end{aligned} \tag{46}$$

where $k_{1x} = 2.6$, $k_{2x} = 6.1$, $k_{3x} = -10.3$, $k_{4x} = -19.2$, $k_{1y} = 3.1$, $k_{2y} = 6.6$, $k_{3y} = -18.7$, and $k_{4y} = -19.3$ are control gains.

2) ECOF control method

$$\begin{aligned} F_x &= -k_{px}\tanh(\phi_x) - k_{dx}\tanh(\xi_x), \\ F_y &= -k_{py}\tanh(\phi_y) - k_{dy}\tanh(\xi_y), \end{aligned} \tag{47}$$

where $\phi_x$, $\xi_x$, $\phi_y$, and $\xi_y$ are defined as follows:

$$\begin{aligned} \phi_x &= x - p_{dx} + \lambda_x S_x C_y, \\ \phi_y &= y - p_{dy} + \lambda_y S_y, \end{aligned} \tag{48}$$

$$\begin{aligned} \xi_x &= \mu_x + k_{dx}\phi_x,\ \dot{\mu}_x = -k_{dx}(\mu_x + k_{dx}\phi_x), \\ \xi_y &= \mu_y + k_{dy}\phi_y,\ \dot{\mu}_y = -k_{dy}\left(\mu_y + k_{dy}\phi_y\right), \end{aligned} \tag{49}$$

and $k_{px} = 13$, $k_{dx} = 2.5$, $k_{py} = 18.3$, $k_{dy} = 5$, $\lambda_x = -5.3$, and $\lambda_y = -2.1$ are control gains.

3) APD-SMC method

$$\begin{aligned} F_x &= -k_{dx}s_1 - k_{px}\int_0^t s_1 d\tau - k_{s1}\tanh(s_1) + \boldsymbol{\varpi}_x\hat{\boldsymbol{P}}_x, \\ F_y &= -k_{dy}s_2 - k_{py}\int_0^t s_2 d\tau - k_{s2}\tanh(s_2) + \boldsymbol{\varpi}_y\hat{\boldsymbol{P}}_y, \end{aligned} \tag{50}$$

where $s_1$ and $s_2$ represent the following sliding surface:

$$\begin{aligned} s_1 &= \dot{x} - \lambda S_x C_y - \alpha_1\dot{\theta}_x, \\ s_2 &= \dot{y} + \gamma S_y - \alpha_2\dot{\theta}_y, \end{aligned} \tag{51}$$

$\boldsymbol{\varpi}_x$ and $\boldsymbol{\varpi}_y$ denote the following variables:

$$\begin{aligned} \boldsymbol{\varpi}_x &= \left[-\lambda\left(\dot{\theta}_x C_x C_y - \dot{\theta}_y S_x S_y\right)\ -\tanh\left(\tfrac{\dot{x}}{\varepsilon_x}\right)\ |\dot{x}|\dot{x}\right]^T, \\ \boldsymbol{\varpi}_x &= \left[-\lambda C_x C_y\left(\dot{\theta}_x C_x C_y - \dot{\theta}_y S_x S_y\right)\ -\tanh\left(\tfrac{\dot{y}}{\varepsilon_y}\right)\ |\dot{y}|\dot{y}\right]^T, \end{aligned} \tag{52}$$

$\hat{\boldsymbol{P}}_x$ and $\hat{\boldsymbol{P}}_y$ are generated by the following update laws:

$$\begin{aligned} \dot{\hat{P}}_x &= -\boldsymbol{\sigma}_x^{-1}\boldsymbol{\varpi}_x s_1, \\ \dot{\hat{P}}_y &= -\boldsymbol{\sigma}_y^{-1}\boldsymbol{\varpi}_x s_2, \end{aligned} \tag{53}$$

the initial values of $\hat{\boldsymbol{P}}_x$ and $\hat{\boldsymbol{P}}_y$ are set as $\mathbf{0}$, and $k_{px} = 3.6$, $k_{dx} = 2.1$, $k_{s1} = 1.5$, $\boldsymbol{\sigma}_x = \boldsymbol{\sigma}_y = diag(5,\ 5,\ 5)$, $\alpha_1 = \alpha_2 = 2$,$\lambda = 4$,$\gamma = 3$, $k_{py} = 2.8$, $k_{dy} = 2.1$, and $k_{s2} = 2$ are control gains,

To better present the superior control performance of the proposed PD-SMC method, the following three performance indices are defined:

a) $\theta_{xmax}$, $\theta_{ymax}$: maximum payload swing amplitude.
b) $\theta_{xres}$, $\theta_{yres}$: residual swing defined as maximum payload swing amplitude after the trolley stops.
c) $\delta_x$, $\delta_y$: positioning error of the trolley after the trolley stops.

**Table 1**
Performance indices of Experiment 1.

| Controllers | $\theta_{xmax}$(deg) | $\theta_{ymax}$(deg) | $\theta_{xres}$(deg) | $\theta_{yres}$(deg) | $\delta_x$(m) | $\delta_y$(m) |
|---|---|---|---|---|---|---|
| LQR controller | 3.3 | 3.0 | 0.9 | 0.8 | 0.001 | 0.002 |
| ECOF controller | 2.7 | 2.5 | 0.3 | 0.2 | 0.003 | 0.001 |
| APD-SMC controller | 2.9 | 3.4 | 0.2 | 0.2 | 0.001 | 0.001 |
| Proposed controller | 1.2 | 1.4 | 0.1 | 0.1 | 0.002 | 0.001 |

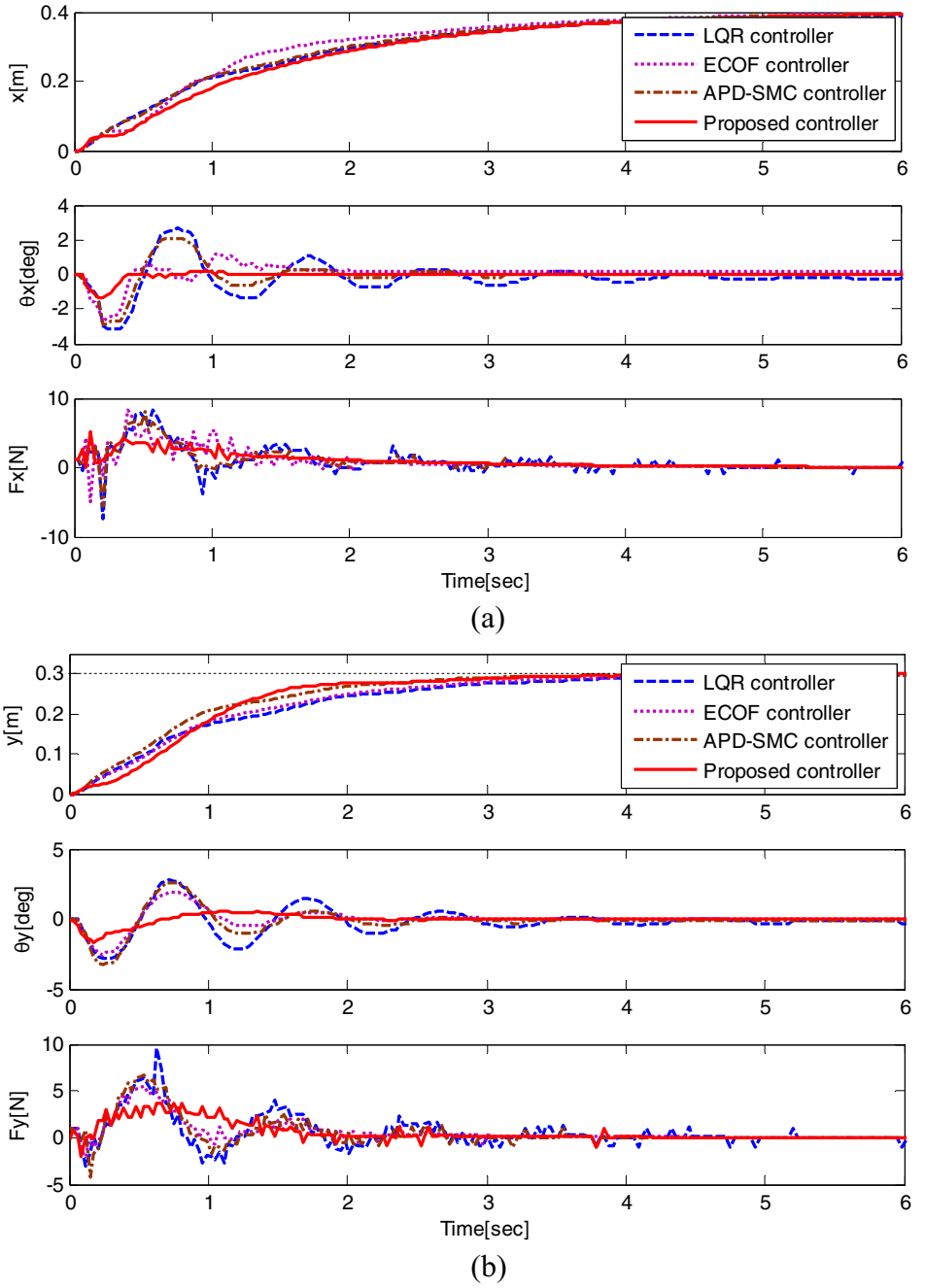


**Fig. 4.** Experimental results for Experiment 1.

Table 1 and Fig. 4 depict the experimental results of the LQR method, the ECOF method, the APD-SMC method, and the proposed method. One can see that, for all the four controllers, the trolley is positioned to the destination within 5 s, with trolley positioning errors less than 3 mm in the *X* axis, and 2 mm in the *Y* axis, respectively. It is seen that the proposed PD-SMC method suppresses and eliminates the payload swing within a smaller range ($\theta_{xmax}$: 1.2 deg, $\theta_{ymax}$: 1.4 deg, and almost no residual payload swing angle) than the LQR controller ($\theta_{xmax}$: 3.3 deg, $\theta_{ymax}$: 3.0 deg, $\theta_{xres}$: 0.9 deg, $\theta_{yres}$: 0.8 deg), the ECOF controller ($\theta_{xmax}$: 2.7 deg, $\theta_{ymax}$: 2.5 deg, and almost no residual payload swing angle), and the APD-SMC method ($\theta_{xmax}$: 2.9 deg, $\theta_{ymax}$: 3.4 deg, and almost no residual payload swing angle). $\theta_{xmax}$ and $\theta_{ymax}$ of the suggested method account for only 36.36% and 46.67% of those corresponding to the LQR controller, respectively, 44.44% and 56% of those corresponding to the ECOF controller, respectively, 41.38% and 41.18% of those corresponding to the APD-SMC method, respectively. In addition,

in the process of transportation, the payload continues swinging back and forth for the LQR method and the APD-SMC method, while the payload is much more steady for the proposed control method and the ECOF method. It can be concluded that the designed controller achieves superior control performance in the sense of payload suppression and elimination.

### *4.2. Experiment 2*

In Experiment 2, the APD-SMC method is still chosen as the comparison method. To further verify the robustness of the proposed method, we consider the following two cases.

Case 1: The payload mass and the cable length are changed to 2 kg and 0.8 m, respectively, while their nominal values are still kept the same as those in experiment 1.

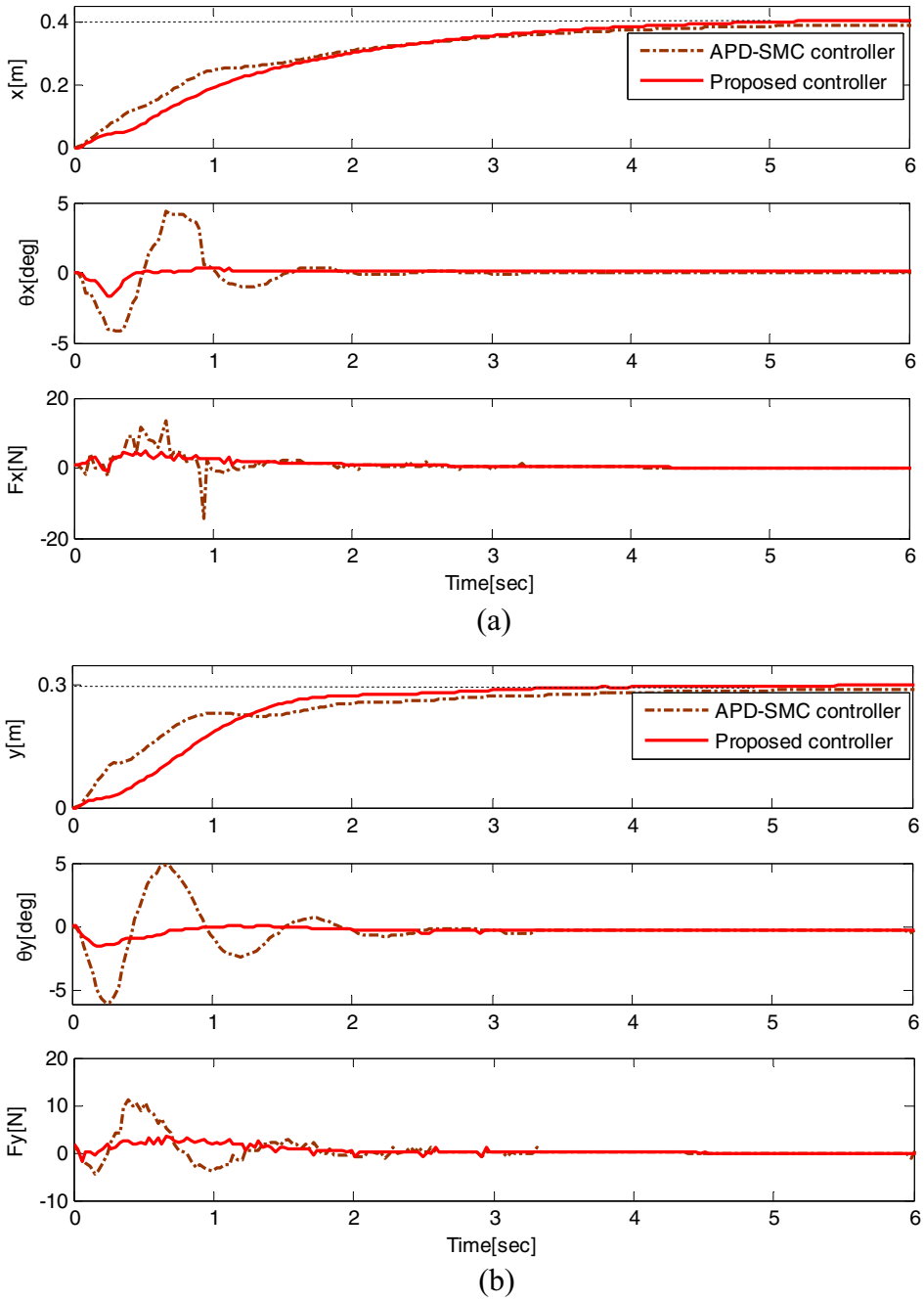


**Fig. 5.** Experimental results for Experiment 2: Case 1.

Case 2: Extra external disturbances are added to the payload swing.

The control gains for the above two cases are kept the same as those in Experiment 1. Figs. 5 and 6 give the experimental results of the APD-SMC method and the suggested method under different uncertainties and external disturbances. By comparing Fig. 5 with 4, although there is much differences between the actual values and nominal values of the cable lengths and the payload masses, the designed controller's transient control performance, especially the payload swing suppression effects, are almost the same whereas those of the APD-SMC method degrade significantly (see the payload swing curves in Figs. 5 and 4). These experimental results demonstrate the strong robustness of the designed controller over uncertain system parameters.

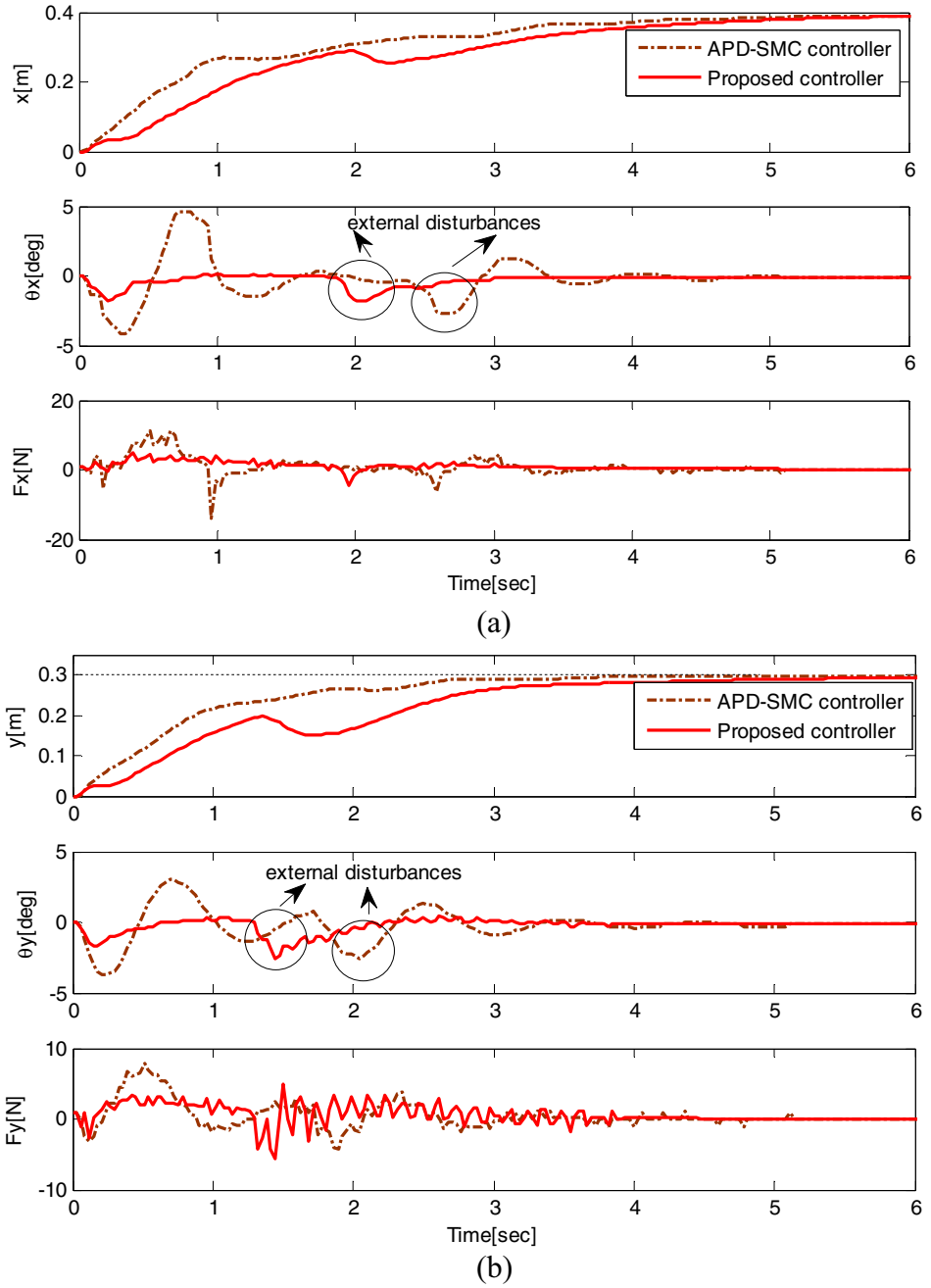


**Fig. 6.** Experimental results for Experiment 2: Case 2.

One can observe from Fig. 6 that the proposed controller has the faster ability to attenuate and damp out the external disturbances than the APD-SMC method, which shows strong robustness of the proposed control method with respect to external disturbances.

## 5. Conclusions

Overhead cranes are often subject to external disturbances and parametric uncertainties in practical applications. Moreover, unmodeled uncertainties, which are hard to be described by accurate mathematical expressions, always exist. To tackle the above mentioned practical problems, a new model-independent anti-swing control law is proposed for 3D overhead crane systems in this work. The designed controller is composed of three parts: the PD part is utilized to stabilize the controlled system; the semi-continuous SMC part is used to provide the strong robustness with respect to external disturbances, parametric and unmodeled uncertainties; the swing-elimination part is used to obtain rapid payload swing suppression and elimination. The stability and convergence are confirmed by Lyapunov-like analysis and Schur component. Our works in the future will mainly focus on designing a PD-SMC method for double- pendulum overhead cranes.

## Acknowledgements

This paper was supported by the Natural Science Foundation of China under Grant 61803174.

## Appendix A. Supplementary data

Supplementary data to this article can be found online at https://doi.org/10.1016/j.ymssp.2019.04.046.

## References

[1] H. Ouyang, X. Deng, H. Xi, J. Hu, G. Zhang, L. Mei, "Novel robust controller design for load sway reduction in double-pendulum overhead cranes," Proceedings of the Institution of Mechanical Engineers, Part C: Journal of Mechanical Engineering Science, in press, doi: 10.1177/0954406218813383.
[2] N. Sun, T. Yang, H. Chen, Y. Fang, Y. Qian, "Adaptive anti-swing and positioning control for 4-DOF rotary cranes subject to uncertain/unknown parameters with hardware experiments," IEEE Transactions on Systems, Man, and Cybernetics: Systems, in press, doi: 10.1109/TSMC.2017.2765183.
[3] N. Sun, Y. Fang, H. Chen, Y. Fu, B. Lu, Nonlinear stabilizing control for ship-mounted cranes with ship roll and heave movements: design, analysis, and experiments, IEEE Trans. Syst., Man, Cybern.: Syst. 48 (10) (2018) 1781–1793.
[4] I. Golovin, S. Palis, Robust control for active damping of elastic gantry crane vibrations, Mech. Syst. Signal Process. 121 (2019) 264–278.
[5] N. Sun, Y. Wu, H. Chen, Y. Fang, An energy-optimal solution for transportation control of cranes with double pendulum dynamics: design and experiments, Mech. Syst. Signal Process. 102 (2018) 87–101.
[6] H. Pan, X. Jing, W. Sun, Z. Li, Analysis and design of a bioinspired vibration sensor system in noisy enviorment, IEEE-ASME Trans. Mechatron. 23 (2) (2018) 845–855.
[7] J. Wu, H.R. Karimi, P. Shi, Network-based H-infinity feedback control for uncertain stochastic systems, Inf. Sci. 232 (2013) 341–397.
[8] Z. Wu, X. Xia, Optimal motion planning for overhead cranes, IET Control Theory Appl. 8 (17) (Nov. 2014) 133–1842.
[9] W. Blajer, K. Kolodziejczyk, Motion planning and control of gantry cranes in cluttered work environment, IET Control Theory Appl. 1 (5) (2007) 1370–1379.
[10] D. Chwa, Nonlinear tracking control of 3-D overhead cranes against the initial swing angle and the variation of payload weight, IEEE Trans. Control Syst. Technol. 17 (4) (2009) 876–883.
[11] N. Sun, T. Yang, Y. Fang, Y. Wu, H. Chen, "Transportation control of double-pendulum cranes with a nonlinear quasi-PID scheme: Design and experiments," IEEE Transactions on Systems, Man, and Cybernetics: Systems, in press, DOI: 10.1109/TSMC.2018.2871627.
[12] L. Ramli, Z. Mohamed, H.I. Jaafar, A neural network-based input shaping for swing suppression of an overhead crane under payload hoisting and mass variations, Mech. Syst. Sig. Process. 107 (2018) 484–501.
[13] H.I. Jaafar, Z. Mohamed, M.A. Shamsudin, N.A.M. Subha, L. Ramli, A.M. Abdullahi, Model reference command shaping for vibration control of multimode flexible systems with application to a double-pendulum overhead crane, Mech. Syst. Sig. Process. 115 (2019) 677–695.
[14] W. Singhose, L. Porter, M. Kenison, E. Kriikku, Effects of hoisting on the input shaping control of gantry cranes, Control Eng. Pract. 8 (10) (2000) 1159–1165.
[15] J. Vaughan, D. Kim, W. Singhose, Control of tower cranes with double-pendulum payload dynamics, IEEE Trans. Control Syst. Technol. 18 (6) (2010) 1345–1358.
[16] D. Fujioka, W. Singhose, Optimized input-shaped model reference control on double-pendulum system, J. Dyn. Syst. Meas. Control-Trans. ASME 140 (10) (2018) 101004.
[17] D. Fujioka, W. Singhose, Input-shaped model reference control of a nonlinear time-varying double-pendulum crane, in: Proc. 10th Asian Control Conf., Kota Kinabalu, Sabah, Malaysia, 2015, pp. 1–6.
[18] D. Fujioka, W. Singhose, Performance comparison of input-shaped model reference control on an uncertain flexible system, in: Proc. IFAC Workshop on Time Delay Syst., Ann Arbor, Michigan, 2015, pp. 129–134.
[19] C. Chang, H. Lie, Real-time visual tracking and measurement to control fast dynamics of overhead cranes, IEEE Trans. Ind. Electron. 59 (3) (2012) 1640–1649.
[20] L.H. Lee, C.H. Huang, S.C. Ku, Z.H. Yang, C.Y. Chang, Efficient visual feedback method to control a three-dimensional overhead crane, IEEE Trans. Ind. Electron. 61 (8) (2014) 4073–4083.
[21] H. Park, D. Chwa, K.S. Hong, A feedback linearization control of container cranes: varying rope length, Int. J. Control Autom. Syst. 5 (4) (2007) 379–387.
[22] N. Uchiyama, Robust control of rotary crane by partial-state feedback with integrator, Mechatronics 19 (8) (2009) 1294–1302.
[23] L.A. Tuan, S.G. Lee, V.H. Dang, S. Moon, B. Kim, Partial feedback linearization control of a three-dimensional overhead crane, Int. J. Control Autom. Syst. 11 (4) (2013) 718–727.
[24] X. Wu, X. He, Partial feedback linearization control for 3-D underactuated overhead crane systems, ISA Trans. 65 (2016) 361–370.
[25] M. Hamdy, R. Shalaby, M. Sallam, A hybrid partial feedback linearization and deadbeat control scheme for a nonlinear gantry crane, J. Inst.-Eng. Appl. Math. 355 (14) (2018) 6286–6299.
[26] Y. Qian, Y. Fang, B. Lu, Adaptive robust tracking control for an offshore ship-mounted crane subject to unmatched sea wave disturbances, Mech. Syst. Sig. Process. 114 (2019) 556–570.

[27] N. Sun, Y. Fang, X. Zhang, Energy coupling output feedback control of 4-DOF underactuated cranes with saturated inputs, Automatica 49 (5) (2013) 1318–1325.
[28] N. Sun, Y. Wu, H. Chen, Y. Fang, "Antiswing cargo transportation of underactuated tower crane systems by a nonlinear controller embedded with an integral term," IEEE Transactions on Automation Science and Engineering, in press, DOI: 10.1109/TASE.2018.2889434.
[29] M. Zhang, "Finite-time model-free trajectory tracking control for overhead cranes subject to model uncertainties, parameter variations and external disturbances," Transactions on the Institute of Measurement and Control, in press, DOI: 10.1177/0142331219830-157
[30] Z. Zhang, Y. Wu, J. Huang, Differential-flatness-based finite-time anti-swing control of underactuated crane systems, Nonlinear Dyn. 87 (3) (2017) 1749–1761.
[31] Z. Wu, X. Xia, B. Zhu, Model predictive control for improving operational efficiency of overhead crane, Nonlinear Dyn. 79 (4) (2015) 2639–2657.
[32] D. Jolevski, O. Bego, Model predictive control of gantry/bridge crane with anti-sway algorithm, J. Mech. Sci. Technol. 29 (2) (2015) 827–834.
[33] G. Galuppini, L. Magli, D.M. Raimondo, Model predictive control of systems with deadzone and saturation, Control Eng. Pract. 78 (2018) 56–64.
[34] W. Chen, M. Saif, Output feedback controller design for a class of MIMO nonlinear systems using high-order sliding-mode differentiators with application to a laboratory 3-D crane, IEEE Trans. Ind. Electron. 55 (11) (2008) 3985–3997.
[35] Z.N. Masoud, A.H. Nayfeh, Sway reduction on container cranes using delayed feedback controller, Nonlinear Dyn. 34 (3–4) (2003) 347–358.
[36] T. Erneux, T. Kalmár-Nagy, Nonlinear stability of a delayed feedback controlled container crane, J. Vib. Control 13 (5) (2007) 603–616.
[37] N. Sun, Y. Wu, Y. Fang, H. Chen, Nonlinear antiswing control for crane systems with double-pendulum swing effects and uncertain parameters: design and experiments, IEEE Trans. Autom. Sci. Eng. 15 (3) (2018) 1413–1422.
[38] H. Pan, X. Jing, W. Sun, H. Gao, A bioinspired dynamics-based adaptive tracking control for nonlinear suspension systems, IEEE Trans. Control Syst. Technol. 26 (3) (2018) 903–914.
[39] M. Zhang, X. Ma, R. Song, X. Rong, G. Tian, X. Tian, Y. Li, Adaptive proportional-derivative sliding mode control law with improved transient performance for underactuated overhead crane systems, IEEE/CAA J. Automatics Sinica 5 (3) (2018) 683–690.
[40] Y. Wu, N. Sun, Y. Fang, D. Liang, "An increased nonlinear coupling motion controller for underactuated multi-TORA systems: Theoretical design and hardware experimentation," IEEE Transactions on Systems, Man, and Cybernetics: Systems, in press, DOI: 10.1109/TSMC.2017.2723478.
[41] R. Liu, S. Li, S. Ding, Nested saturation control for overhead crane systems, Trans. Inst. Meas. Control 34 (7) (2012) 862–875.
[42] W. Yu, M.A. Moreno-Armendariz, F.O. Rodriguez, Stable adaptive compensation with fuzzy CMAC for an overhead crane, Inf. Sci. 181 (21) (2011) 4895–4907.
[43] Q.H. Ngo, N.P. Nguyen, C.N. Nguyen, T.H. Tran, Q.P. Ha, Fuzzy sliding mode control of an offshore container crane, Ocean Eng. 140 (2017) 125–134.
[44] B. Rong, X. Rui, L. Tao, G. Wang, Dynamics analysis and fuzzy anti-swing control design of overhead crane system based on Riccati discrete time transfer matrix method, Multibody Syst. Dyn. 43 (3) (2018) 279–295.
[45] L. Tuan, H.M. Cuong, P. Van Trieu, L.C. Nho, V.D. Thuan, L. Anh, Adaptive neural network sliding mode control of shipboard container cranes considering actuator backlash, Mech. Syst. Sig. Process. 112 (2018) 233–250.
[46] D. Liu, J. Yi, D. Zhao, W. Wang, Adaptive sliding mode fuzzy control for a two-dimensional overhead crane, Mechatronics 15 (5) (2005) 505–522.
[47] N.B. Almutairi, M. Zribi, Sliding mode control of a three-dimensional overhead crane, J. Vib. Control 15 (11) (2009) 1679–1730.
[48] A.T. Le, S.G. Lee, L.C. Nho, H.K. Dong, Model reference adaptive sliding mode control for three-dimensional overhead cranes, Int. J. Precis. Eng. Manuf. 14 (8) (2013) 1329–1338.
[49] N. Sun, Y. Fang, H. Chen, A new antiswing control method for underactuated cranes with unmodeled uncertainties: theoretical design and hardware experiments, IEEE Trans. Ind. Electron. 62 (1) (2015) 453–465.
[50] H. Pan, X. Jing, W. Sun, Robust finite-time tracking control for nonlinear suspension systems via disturbance compensation, Mech. Syst. Sig. Process. 88 (2017) 49–61.
[51] D. Chwa, Sliding-mode-control-based robust finite-time antisway tracking control of 3-D overhead cranes, IEEE Trans. Ind. Electron. 64 (8) (2017) 6775–6784.
[52] B. Siciliano, L. Sciavicco, L. Villani, G. Oriolo, Robotics: Modeling, Planning and Control, Springer Verlag, 2009.
[53] M.W. Spong, M. Vidyasagar, Robot Dynamics and Control, Wiley, New York, 1989.
[54] P. Ouyang, J. Acob, V. Pano, PD with sliding mode control for trajectory tracking of robotic system, Rob. Comput. Integr. Manuf. 30 (2) (2014) 189–200.
[55] W. Yue, V. Pano, P. Ouyang, Y. Hu, Model-independent position domain sliding mode control for contour tracking of robotic manipulator, Int. J. Syst. Sci. 48 (1) (2017) 190–199.
[56] S. Boyd, L. Vandenberghe, Convex Optimization, Cambridge University Press, Cambridge, Ny, USA, 2004.
[57] H.K. Khalil, Nonlinear Systems, 3rd edn., Prentice-Hall, 2002.